Journal of Alloys and Compounds 923 (2022) 166364

Contents lists available at ScienceDirect

Journal of Alloys and Compounds

journal homepage: www.elsevier.com/locate/jalcom

Effect of Gd on the microstructure and mechanical properties of high-pressure die-cast Mg-La-Ce alloys at ambient and elevated temperatures

Lingyun Feng[a], Xixi Dong[a,*], Qing Cai[a], Bin Wang[b], Shouxun Ji[a]

[a] Brunel Centre for Advanced Solidification Technology (BCAST), Brunel University London, Uxbridge Middlesex UB8 3PH, United Kingdom
[b] Department of Mechanical Engineering and Aerospace, Brunel University London, Uxbridge Middlesex UB8 3PH, United Kingdom

ARTICLE INFO

Article history:
Received 30 April 2022
Received in revised form 29 June 2022
Accepted 18 July 2022
Available online 20 July 2022

Keywords:
Magnesium alloys
Microstructures
Mechanical properties
Strengthening mechanism
Elevated temperatures

ABSTRACT

The microstructure and tensile properties of die-cast Mg-1.6 wt%La-1.0 wt%Ce alloys with Gd content ranging from 0 wt% to 3.0 wt% were investigated. The major intermetallic compound formed at the grain boundaries of the alloys was the skeleton-like $Mg_{12}RE$ phase, and the domains of {011} twins can be observed in $Mg_{12}RE$. Three minor intermetallic compounds formed at the grain boundaries of the alloys with Gd addition, i.e., the irregular-shaped Mg_2Gd phase, the needle-like Mg_3Gd phase and the blocky Gd-Mn phase. The addition of Gd resulted in the increase of yield strength (YS) at both ambient and elevated temperatures. The YS of the Gd-free alloy was 135.3 MPa at ambient temperature and 57.3 MPa at 300 °C. The YS of the alloy with 3.0 wt% Gd was 162.1 MPa at ambient temperature and 97.3 MPa at 300 °C, which were increased by 19.8 % and 69.8 %, respectively, in contrast to the alloy without Gd addition. The addition of Gd increased the volume fraction of intermetallic compounds from 11.7 % to 18.5 %, while it had a very limited effect on the grain size of the Mg matrix phase. The increase in ambient YS can be mainly attributed to the increased secondary phase strengthening of intermetallic compounds at grain boundaries and the enhanced solid solution strengthening of Gd in the Mg matrix. The increased volume fraction of thermally stable intermetallic compounds $Mg_{12}RE$, Mg_2Gd and Mg_3Gd contributed to the increase of YS at elevated temperatures. The fracture mechanism of the Gd-containing alloys at ambient temperature was a quasi-cleavage fracture.

1. Introduction

Magnesium (Mg) alloy is a promising light alloy due to its high specific strength, specific stiffness, and low density [1–3]. It has been used in transportation, aerospace, electronics, and other industrial fields. To achieve high productivity and low mass-production cost, most of the applied Mg alloys are made by high-pressure die casting (HPDC) [4,5]. However, the further application of Mg alloys is partly limited by the poor plasticity at ambient temperature and the low heat resistance at elevated temperatures, especially for working temperatures above 200 °C [6]. Recently, emerging markets such as engines in powered tools and drones, battery packs and electric motors in electric vehicles require high-performance heat-resistant die-cast Mg alloys [7,8]. There is a great need to develop die-cast Mg alloys with good mechanical properties at a temperature above 200 °C.

Alloying is a common method to improve the mechanical properties of Mg alloys. Appropriate alloying elements were introduced to achieve alloy strengthening by utilizing strengthening mechanisms such as grain size, secondary phase, solid solution and precipitation strengthening [9,10]. The effects of alloying elements, such as Al, Zn, Mn, Ca, and rare earth (RE), on the microstructure and mechanical properties of Mg alloys have been widely studied [2,11–15]. The most widely used die-cast Mg alloys are Mg-Al series alloys, such as AZ91, AM50 and AE44 [3]. However, the $Mg_{17}Al_{12}$ phase, which formed in die-cast Mg-Al series alloys, cannot nail the grain boundaries (GBs) effectively at elevated temperatures, thus deteriorating the creep properties and reducing the high-temperature strength of the alloys [16]. Wang et al. [17] studied the Ca-added AZ91 alloy and found that the partial replacement of the $Mg_{17}Al_{12}$ phase by the Al_2Ca phase increased the YS at 150 °C. Nakaura et al. [18] studied the AC515 alloy and found that the addition of Sr led to the formation of a thermally stable Al-Sr phase, which improved the strength at 150 °C. In addition, RE elements have also been applied to enhance the high-temperature mechanical properties of Mg-Al-based alloys [3]. Hu et al. [19] improved the strength of the Mg-5Al-

* Corresponding author.
E-mail address: Xixi.Dong@brunel.ac.uk (X. Dong).

https://doi.org/10.1016/j.jallcom.2022.166364
0925-8388/

2Si alloy at 150 °C by adding Ce. Zhang et al. [20] studied the AM40-xCe alloy and found that with increasing Ce addition, the $Al_{11}Ce_3$ phase gradually replaced the $Mg_{17}Al_{12}$ phase, resulting in a gradual increase in the high-temperature strength of the alloy. It was reported that the addition of Nd to the AM40 alloy can effectively suppress the $Mg_{17}Al_{12}$ phase, and the formation of Al_2Nd and $Al_{11}Nd_3$ phases can improve the high-temperature strength of the alloy [21]. Zhu et al. [22] studied the AE44 alloy and found that the La element had a more effective enhancement of the high-temperature strength compared with the RE elements of Ce and Nd. Although a considerable number of high-pressure die-cast Mg-Al-based alloys have been developed, most of these alloys can only work below 200 °C due to the presence of thermally unstable intermetallic compounds [23]. For the gravity casting Mg-RE alloys without Al elements, such as WE43 and Elektron 21, which can be applied in a working environment above 200 °C, however, these alloys are not suitable for HPDC due to the hot-tearing [24].

In the past two decades, several Al-free Mg-RE alloys that are suitable for HPDC have been developed for application in high-temperature environment. The benchmark die-cast Mg-2.5RE-0.35Zn (MEZ) alloy has good creep performance due to the formation of a thermally stable $Mg_{12}RE$ phase, but the strength of the alloy at ambient and elevated temperatures is low [25]. The other benchmark Mg-4 wt%RE (La, Ce, Nd) (HP2 +) alloy can offer good strength and creep properties up to 200 °C [24]. According to the current research status of Al-free die-cast Mg-RE alloys, it can be found that the RE alloying mostly focuses on light RE elements such as La, Ce and Nd. In addition, it is believed that the addition of Gd and Y to Mg-La alloys can improve the castability of the alloys relative to Nd, while the addition of Nd contributes more to the grain boundary strengthening of the alloys in comparison to Gd and Y [26]. Although there have been partial reports on the brief study of the microstructure and room temperature mechanical properties of Gd-added die-cast Mg-RE alloys [27–30], there have been few detailed studies about the effect of Gd on the formation of intermetallic phases especially Gd-containing compounds and the high-temperature mechanical properties of die-cast Mg-RE alloys.

The aim of this work is to investigate the effect of Gd on the microstructure and mechanical properties of the high-pressure die-cast Mg1.6La1Ce-xGd (x = 0–3, compositions in the text are in wt% unless specified) alloys at ambient temperature and elevated temperatures of 250 °C and 300 °C. This paper also discussed the strengthening and fracture mechanisms and the relationship between microstructure and mechanical properties of the alloys.

2. Experimental

2.1. Preparation of alloy melts and HPDC

Mg1.6La1Ce-xGd alloys were made using pure Mg (99.9 wt%), pure zinc (99.5 wt%) and master alloys of Mg–5 wt%Mn, Mg-30 wt% La, Mg-25 wt%Ce and Mg-30 wt%Gd. The desired alloys were melted in a resistance furnace at 720 °C under the protection of a mixture of N_2 and 0.5 % SF_6. After homogenisation and elimination of impurities, the mushroom samples were poured for the measurement of chemical composition by inductively coupled plasma-optical emission spectrometry (ICP-OES), as shown in Table 1.

Die-casting was carried out on a 4500 kN cold chamber high-pressure die casting machine. The melt temperature was measured with a type K thermocouple, then the melt was released into the shot sleeve. The die temperature was 220 °C, and the pouring temperature was 715 °C. Eight tensile test samples with a gauge diameter of 6.35 mm and a gauge length of 50 mm were prepared in each die-casting shot.

Table 1
Chemical composition of experimental Mg1.6La1Ce-xGd alloys obtained by ICP-OES.

Alloy	x	La	Ce	Gd	Zn	Mn	Mg
Mg1.6La1.0Ce-0Gd	x = 0	1.59	0.97	0.01	0.48	0.28	Bal.
Mg1.6La1.0Ce-0.5Gd	x = 0.5	1.54	0.95	0.48	0.46	0.27	Bal.
Mg1.6La1.0Ce-1.0Gd	x = 1	1.54	0.94	0.97	0.47	0.24	Bal.
Mg1.6La1.0Ce-1.5Gd	x = 1.5	1.55	0.94	1.44	0.44	0.27	Bal.
Mg1.6La1.0Ce-2.0Gd	x = 2	1.56	0.96	2.01	0.45	0.25	Bal.
Mg1.6La1.0Ce-3.0Gd	x = 3	1.53	0.94	2.94	0.47	0.27	Bal.

2.2. Tensile tests

Tensile tests were carried out in accordance with ASTM B557–15 and ASTM E8/E8M-16 standards using the Instron 5500 universal electromechanical test system, which was equipped with Bluehill software and a 50 kN load cell. All tests were conducted at ambient temperature (20 °C) and elevated temperatures of 250 °C and 300 °C. Extensometer with a nominal pitch of 50 mm was applied during ambient temperature tensile tests, while elevated temperature tensile tests were conducted without extensometer. The tensile rates of ambient and elevated temperature tensile tests were 1 mm/min and 0.0002/s, respectively. Each reported data was based on a six-sample average.

2.3. Microstructure analysis

The centre portion of the stretch bar was used for microstructural examination. ZEISS SUPRA 35VP scanning electron microscopy (SEM) with energy dispersive X-ray spectroscopy (EDX) was used for Backscatter Electronics (BSE) and Secondary Electronics (SE) morphology observation. SEM analysis was conducted at an accelerated voltage of 20 kV. The 50 μm thick and 3 mm diameter transmission electron microscopy (TEM) samples were thinned using the Gatan Precision Ion Polishing System (PIPS) at a voltage of 3–5 kV and an angle of 3–5°. Thinned TEM samples were used for selected area electron diffraction (SAED), bright-field (BF) and high-resolution TEM (HRTEM) imaging on a JEOL 2100F machine. ImageJ software was used to measure phase volume fraction and grain size. X-ray diffraction (XRD) analysis was conducted on a D8 instrument in the 2 Theta degrees from 20° to 100°.

3. Results

3.1. XRD results

Fig. 1 shows the XRD spectra for the as-cast Mg1.6La1Ce-xGd alloys with different Gd contents. α-Mg and $Mg_{12}RE$ phases were detected in the alloys with the Gd contents that were less than 2.0 wt%. In addition to α-Mg and $Mg_{12}RE$, Mg_3Gd phase can be detected in the alloy with the Gd content of 3.0 wt%. It should be mentioned that phases with small size or small volume fraction are normally hard to be detected under XRD.

3.2. Overall microstructure

Fig. 2 displays the BSE-SEM microstructure of the die-cast Mg1.6La1Ce-xGd alloys in the as-cast state. The Mg1.6La1Ce-xGd alloys comprise the α-Mg matrix phase and the intermetallic phases at GBs. The α-Mg matrix phase shows two different grain sizes, which is typical feature of the die-cast alloys [4]. The α_1-Mg phase with larger grain size nucleated in the shot sleeve with lower cooling rate, and the α_2-Mg phase with smaller grain size nucleated in the die cavity with higher cooling rate. The intermetallic phases at GBs show skeleton-like morphology.

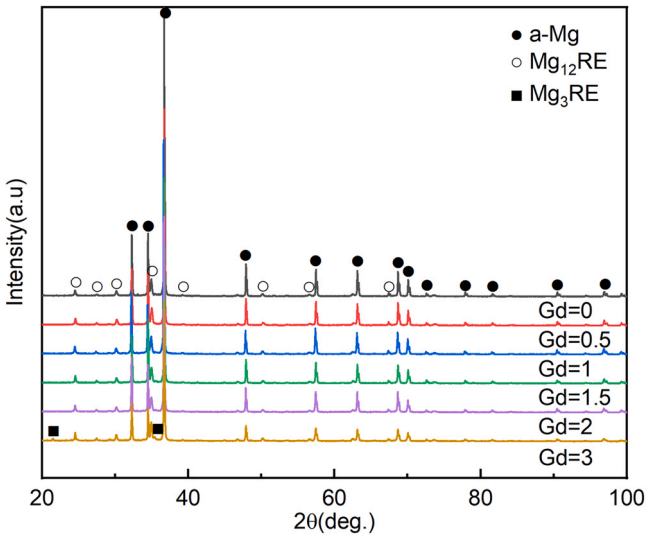

Fig. 1. XRD results of Mg1.6La1Ce-xGd alloys in the as-cast state (x = 0, 0.5, 1.0, 1.5, 2.0, 3.0).

Fig. 3a and b show the statistical grain size of the α-Mg matrix phase and the volume fraction of the intermetallic phase at GBs, respectively, in the die-cast Mg1.6La1Ce-xGd alloys under as-cast condition. The average grain size in the Mg1.6La1Ce alloy was 9.1 μm, with the large grains up to 33 μm. The addition of Gd slightly refined the grain size. The average grain size in the alloy with 1 wt% Gd was 8.6 μm, and the large grains were refined to about 27 μm. However, with the further addition of Gd, the average grain size increased slightly. When 3.0 wt% Gd was added, the grain size of the alloy was 9.2 μm, and the size of large grains was about 29 μm. It is clear that the grain size of the alloys with Gd addition fluctuates, but the variation is not significant. The volume fraction of the intermetallic phase at GBs increased gradually with the addition of Gd, as shown in Fig. 3b.

Fig. 4 displays the high magnification SEM-BSE morphology of the intermetallic phases at GBs of the die-cast Mg1.6La1Ce-xGd alloys in as-cast state. In the absence of Gd addition, the intermetallic phase shows rod-shaped and layered morphology. With the addition of Gd, the fibrous or lamellar morphology of the $Mg_{12}RE$ intermetallic phases became indistinctive, as shown in Fig. 4b–f. In addition, the addition of Gd led to the formation of the minority of small-sized compounds, which was brighter than the major skeleton-like intermetallic phase. With the addition of 3.0 wt%, the small-sized compounds can be clearly observed.

3.3. Determination of intermetallics at GBs

3.3.1. $Mg_{12}RE$ intermetallic phase

Fig. 5 shows a detailed analysis of the major $Mg_{12}RE$ intermetallic phase at GBs of the die-cast Mg1.6La1Ce-3Gd alloy under as-cast condition. The SEM-EDX results in Fig. 5b show that the atomic ratio of Mg:(La, Ce, Gd, Zn) in the major skeleton-like intermetallic phase is approximately 12.7, suggesting a phase of $Mg_{12}RE$. The TEM-SAED pattern in Fig. 5e further confirms that the major skeleton-like

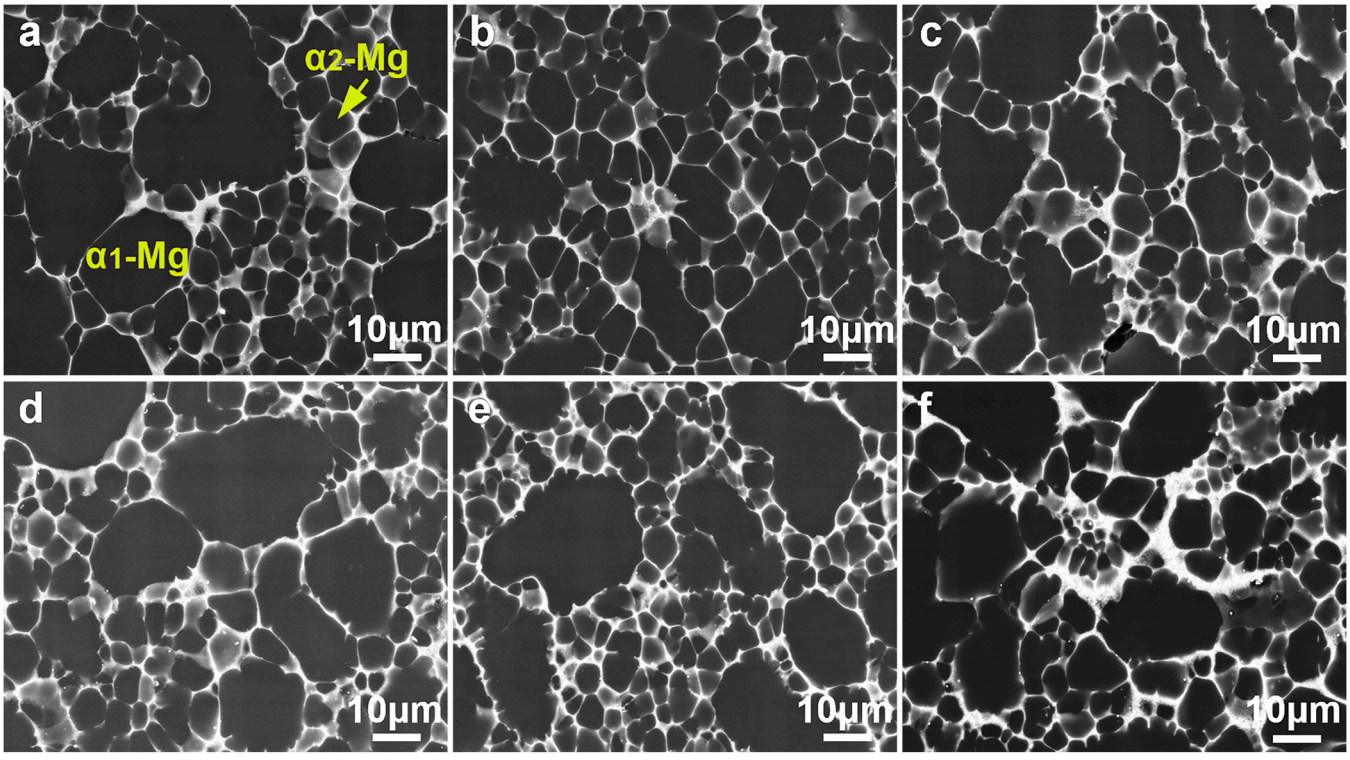

Fig. 2. BSE-SEM microstructure of the die-cast Mg1.6La1Ce-xGd alloys in the as-cast state. (a) x = 0 Gd, (b) x = 0.5 Gd, (c) x = 1.0 Gd, (d) x = 1.5 Gd, (e) x = 2.0 Gd, (f) x = 3.0 Gd.

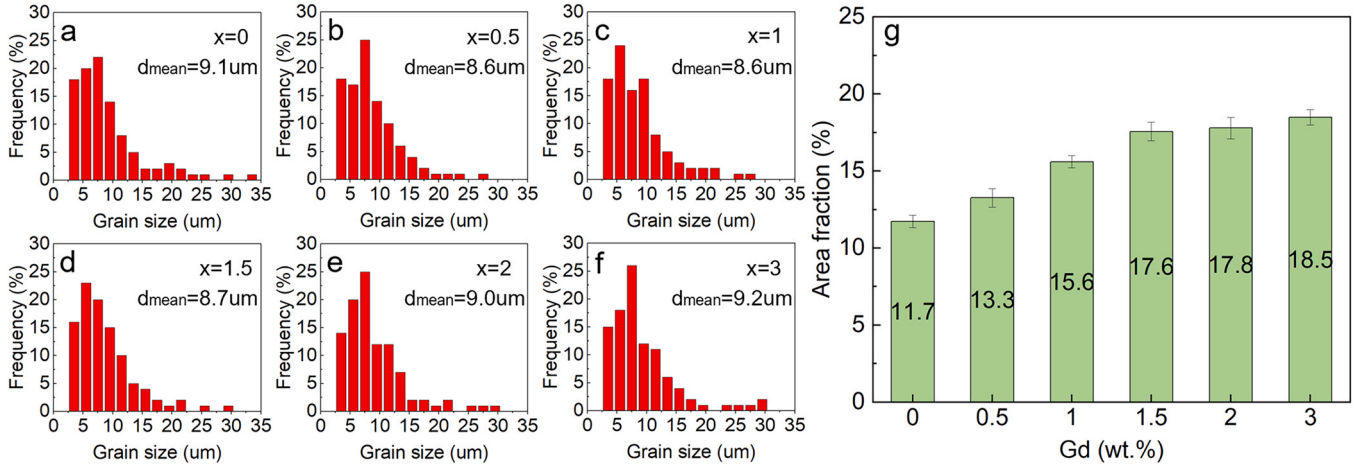

Fig. 3. (a–f) Grain size distribution of Mg matrix phase and (g) volume fraction of the intermetallic phase in the die-cast Mg1.6La1Ce-xGd (x = 0, 0.5, 1.0, 1.5, 2.0, 3.0) alloys under as-cast condition.

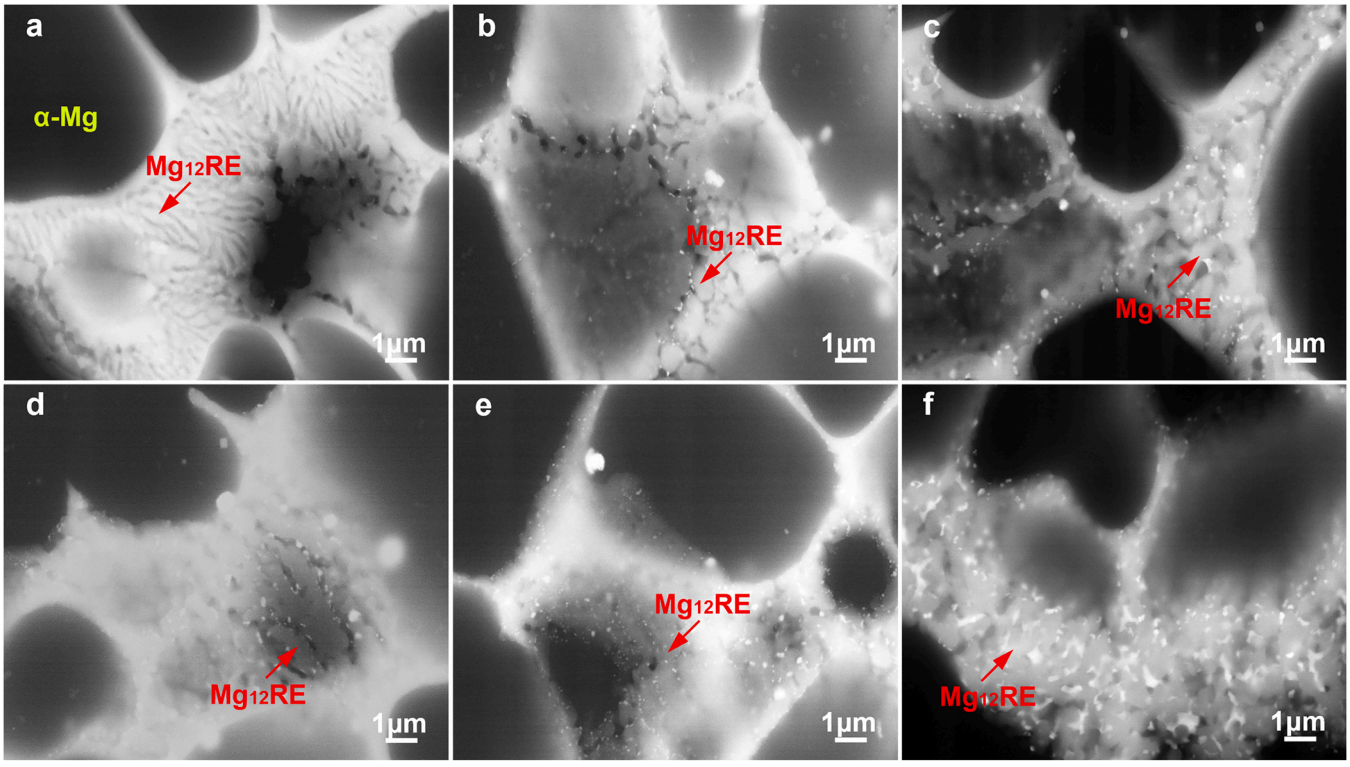

Fig. 4. BSE-SEM microstructure of the die-cast Mg1.6La1Ce-xGd alloys in as-cast state with high magnification. (a) x = 0, (b) x = 0.5, (c) x = 1.0, (d) x = 1.5, (e) x = 2.0, (f) x = 3.0.

intermetallic phase is $Mg_{12}RE$ (body-centred tetragonal, a = 1.033, c = 0.596, I4/mmm) [31], which is consistent with the XRD results in Fig. 1. Additionally, the TEM-SAED pattern in Fig. 5f shows the presence of the local domains of {011} twins in $Mg_{12}RE$. Hua et al. [32] also found the local domains of {101} twins in the $Mg_{12}RE$ phase of the die-cast Mg-4Zn-2La-3Y alloy. The presence of twins has not been reported in previous studies on Mg-La-Ce-Nd alloys [33]. It has been reported that the segregation of Zn elements in the $Mg_{12}RE$

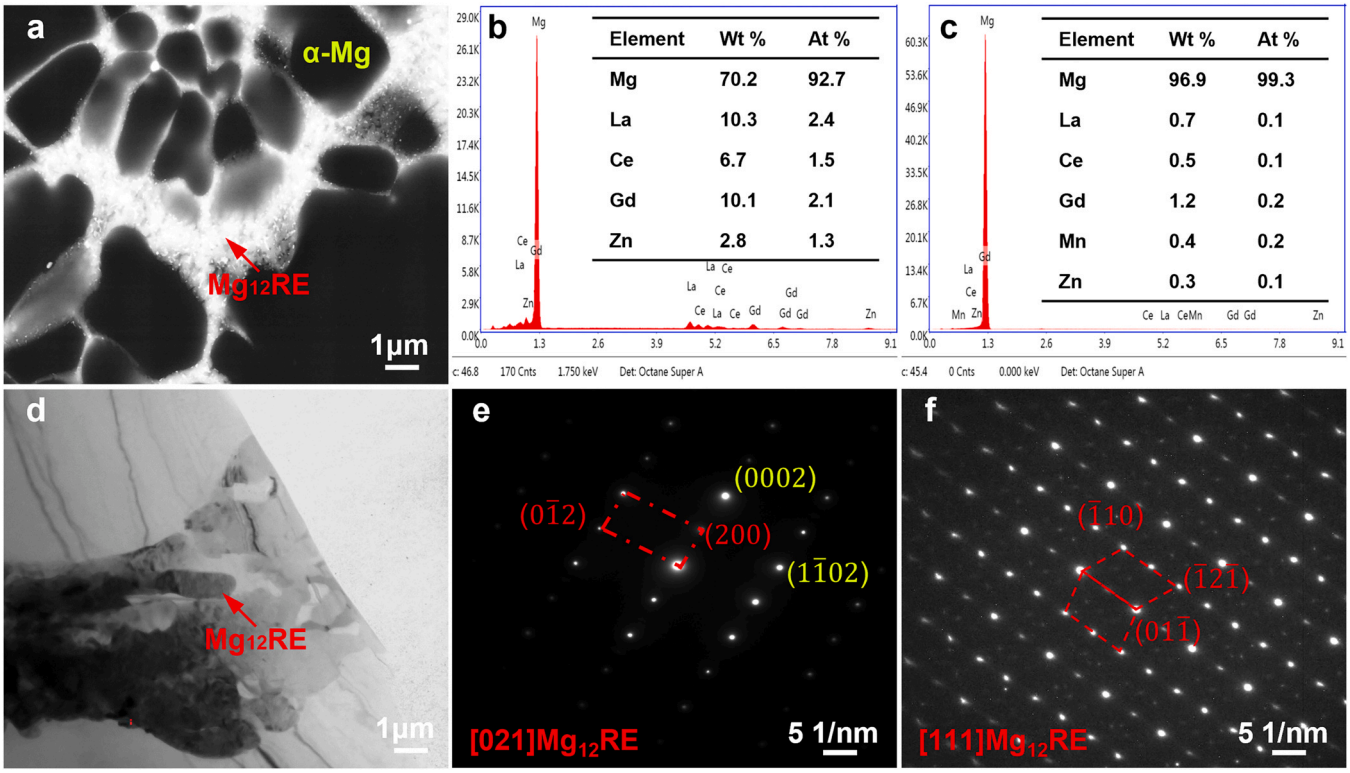

Fig. 5. Microstructure of the major $Mg_{12}RE$ intermetallic phase at grain boundaries of the die-cast Mg1.6La1Ce-3Gd alloy under as-cast condition. (a) High magnification BSE-SEM image; (b) SEM-EDX result of $Mg_{12}RE$ phase; (c) SEM-EDX result of α-Mg; (d) BF-TEM image of $Mg_{12}RE$ phase at GBs; (e,f) SAED of $Mg_{12}RE$ phase observed along [021] and [111] zone axes.

phase decreases the sault fault energy and thus promotes twinning [34]. The SEM-EDX results in Fig. 5b show the considerable presence of Zn in the $Mg_{12}RE$ phase. Therefore, Zn promoted the formation of twins in the $Mg_{12}RE$ phase of the present alloy.

3.3.2. Mg_2Gd intermetallic phase

Fig. 6a displays the TEM morphology of the minor Mg_2Gd and Mg_3Gd intermetallic phases at GBs of the die-cast Mg1.6La1Ce-3Gd alloy under as-cast condition. The Mg_2Gd intermetallic phase was in irregular shape, as indicated by the dashed circle A. Fig. 6b–g shows the STEM-EDX mapping of elements Mg, La, Ce, Gd, Mn and Zn in Fig. 6a, respectively. Fig. 6h shows the STEM-EDX result of point A in Fig. 6a, and the irregular shaped intermetallic phase was rich in Mg, Gd, and Zn, with a Mg:(Gd, Zn) atomic ratio of 2.13, which indicates that the irregular shaped intermetallic phase is Mg_2(Gd, Zn) (face-centred cubic, a = 0.8575, Fd-3m) [35].

Fig. 7 shows the HRTEM images of two Mg_2Gd phases at GBs of the die-cast Mg1.6La1Ce-3Gd alloy in the as-cast state. The Fast Fourier Transform (FFT) patterns in Fig. 7b and e further confirmed the Mg_2Gd phases, and the FFT patterns in Fig. 7c and e further verified that major intermetallic phase adjacent to the Mg_2Gd phases was $Mg_{12}RE$, under the zone axes of $[010]_{Mg2Gd}//[\bar{2}\bar{2}1]_{Mg12RE}$ or $[001]_{Mg2Gd}//[221]_{Mg12RE}$. The lack of detection in XRD should be due to the small content of the Mg_2(Gd, Zn) phase that was hard to be detected.

3.3.3. Mg_3Gd intermetallic phase

As marked by the dashed circle in Fig. 6a, another minor needle-like Mg_3Gd intermetallic phase was observed at GBs of the die-cast Mg1.6La1Ce-3Gd alloy under as-cast condition. The STEM-EDX map in Fig. 6e and the STEM-EDX result in Fig. 6i show that the needle-like intermetallic phase is rich in Gd. Fig. 8b shows the high magnification TEM morphology of the needle-like Mg_3Gd intermetallic phases, and the TEM-SAED patterns in Fig. 8c and d confirmed that the needle-like intermetallic phases were Mg_3Gd (face-centred cubic, a = 0.73, Fm-3m) [28]. It was reported that both Mg_2Gd and Mg_3Gd phases had good thermal stability [29], which were beneficial to the high temperature mechanical properties of Mg alloys.

3.3.4. Gd-Mn intermetallic phase

Fig. 9a displays the TEM morphology of the third minor blocky Gd-Mn intermetallic phase at GBs of the die-cast Mg1.6La1Ce-3Gd alloy under as-cast condition. The STEM-EDX mapping in Fig. 9b–g shows that the blocky Gd-Mn intermetallic phase is rich in Gd, La, Ce

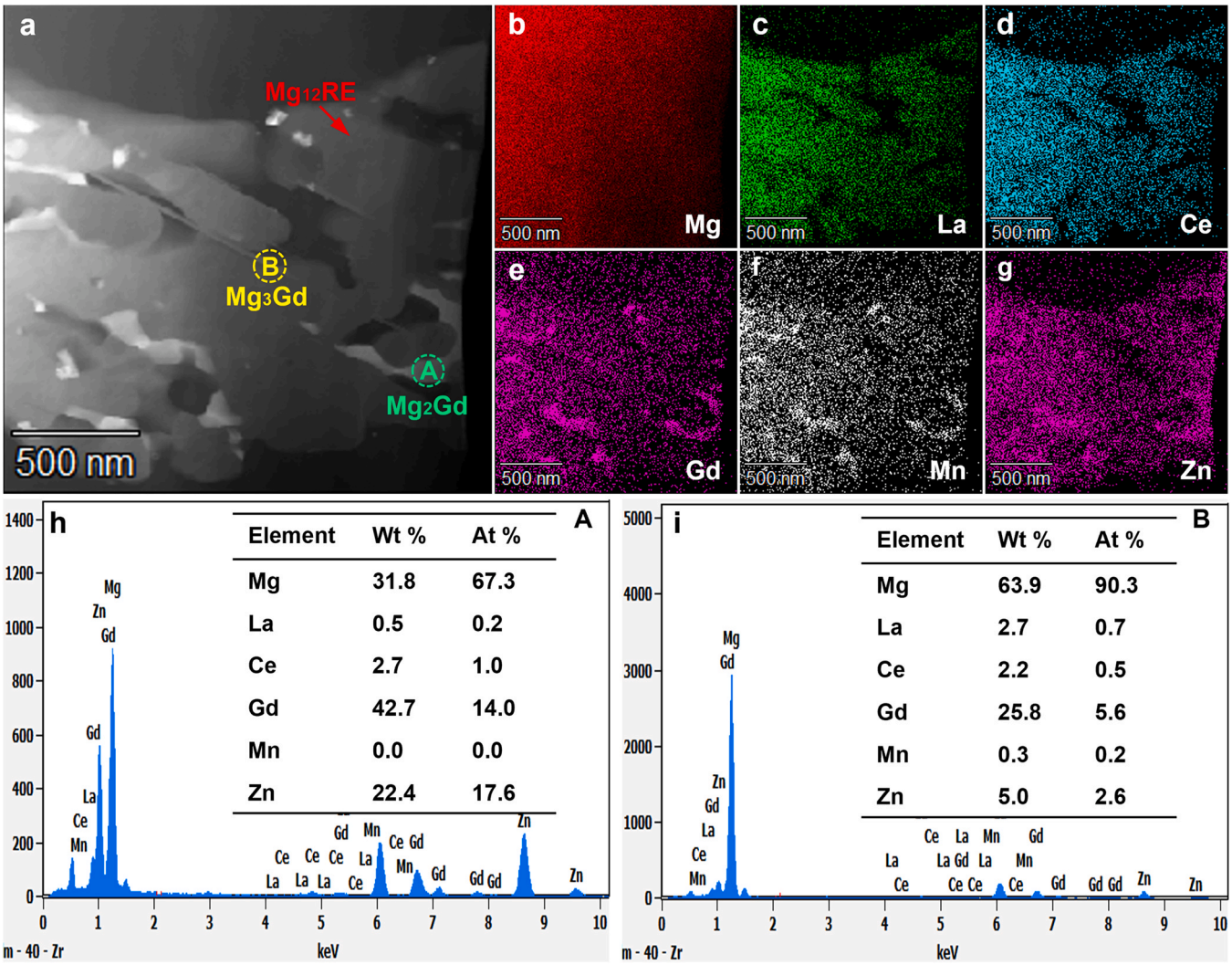

Fig. 6. TEM morphology and STEM-EDX results of the minor Mg_2Gd and Mg_3Gd intermetallic phases at grain boundaries of the die-cast Mg1.6La1Ce-3Gd alloy under as-cast condition. (a) High magnification STEM image; (b–g) STEM-EDX mapping of elements (b) Mg, (c) La, (d) Ce, (e) Gd, (f) Mn and (g) Zn in (a); (h) STEM-EDX result of point A-Mg_2Gd in (a); (i) STEM-EDX result of point B-Mg_3Gd in (a).

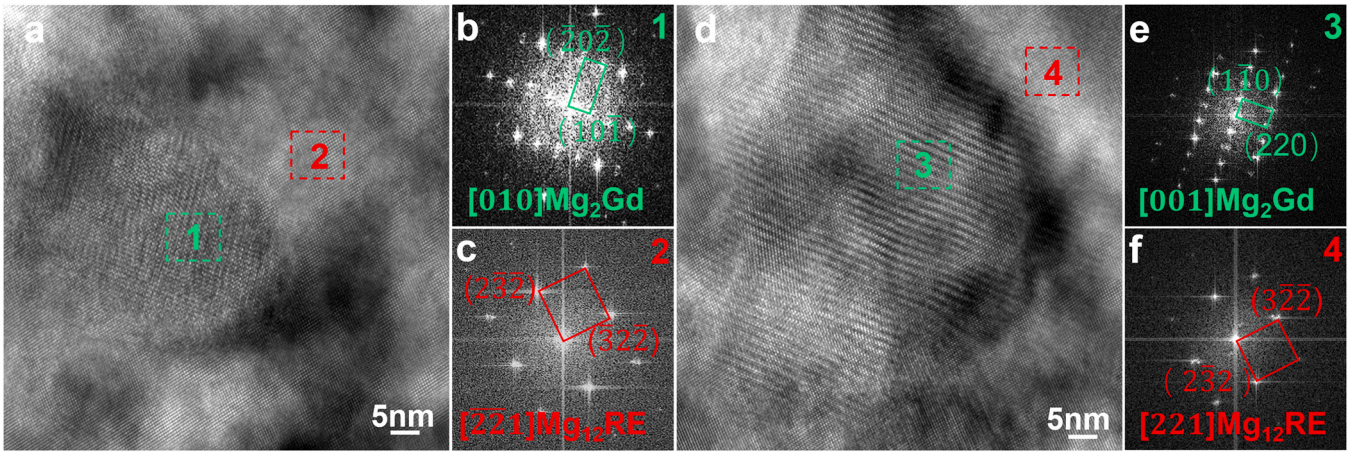

Fig. 7. HRTEM image of two Mg_2Gd phases at the grain boundaries of the die-cast Mg1.6La1Ce-3Gd alloy in the as-cast state. (a) and (d) are HRTEM images of the two Mg_2Gd phases, respectively; (b), (c) and (e), (f) are FFT patterns corresponding to the Mg_2Gd and the adjacent $Mg_{12}RE$ phases.

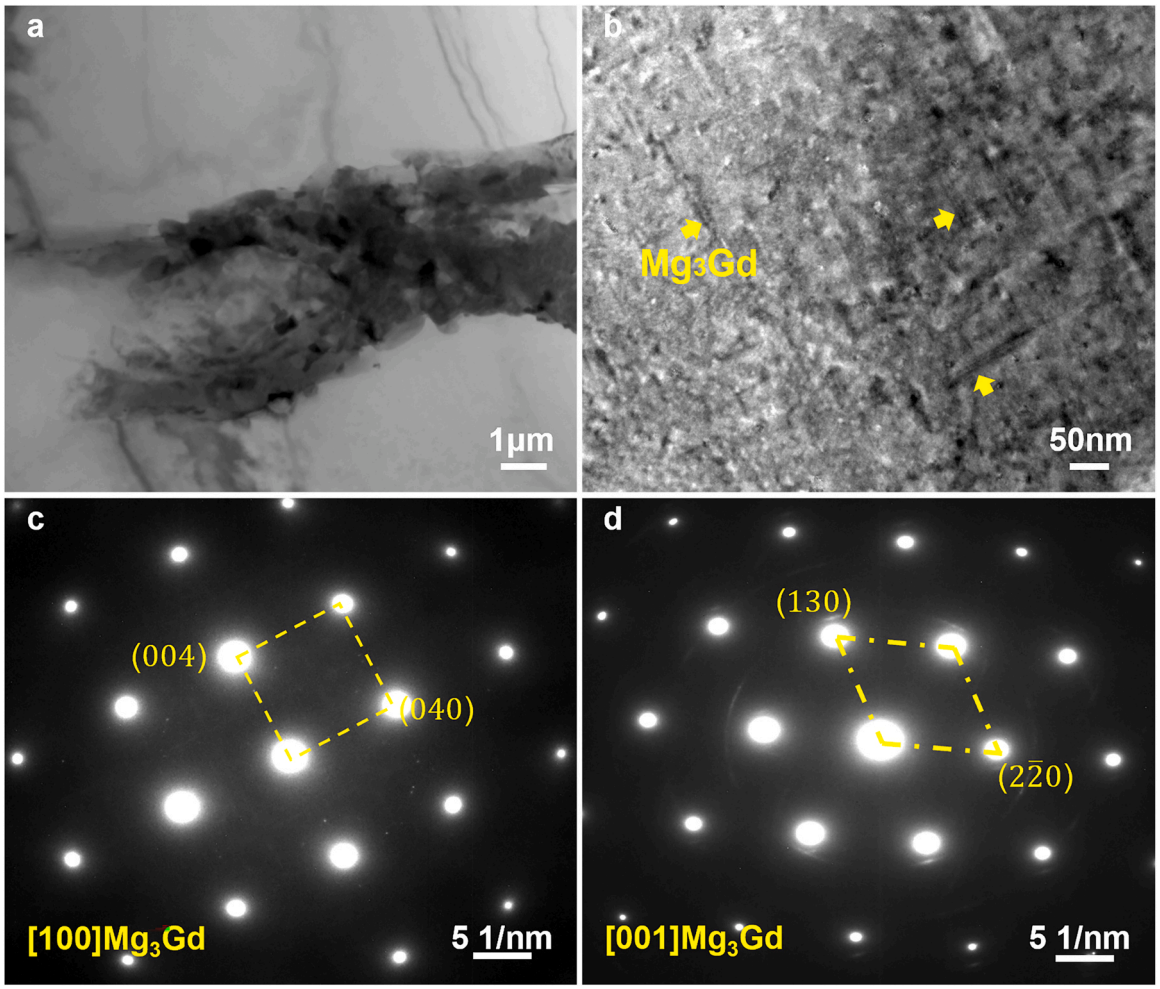

Fig. 8. TEM confirmation of the needle-like Mg_3Gd intermetallic phase at grain boundaries of the die-cast Mg1.6La1Ce-3Gd alloy under as-cast condition. (a) Low magnification BF-TEM image; (b) High magnification BF-TEM image, the yellow arrows mark the needle-like Mg_3Gd phase; (c,d) SAED of Mg_3Gd phases observed along [100] and [001] zone axes.

and Mn. Fig. 9h provides the composition of the Gd-Mn intermetallic phase that was measured by STEM-EDX, and the detected Mn content was relatively low, while the content of Gd was much higher than that of La and Ce. This may be due to the low addition of Mn in the alloy. Previous studies have suggested that rare earth elements such as Gd and Y are prone to solute segregation in cast Mg alloys at defective locations such as boundaries [30,36,37]. The phenomenon of solute segregation is usually due to the atomic size effect [38]. It has also been reported that Mn is prone to co-segregation with Nd and Gd [39,40]. Therefore, the formation of Gd-Mn intermetallic phase might be due to the co-segregation of Gd and Mn elements, which will be investigated in detail in future research.

3.4. Mechanical properties at ambient and elevated temperatures

Figs. 10a–c and 11a–c show the stress-strain curve and tensile properties of die-cast Mg1.6La1Ce-xGd alloys at ambient temperature and elevated temperatures of 250 °C and 300 °C. With the increased addition of Gd, the YS of the alloys increases, while the corresponding elongation (El) decreases at ambient temperature. Compared with the alloy without Gd, the addition of 3.0 wt% Gd led to an increase of 19.8 % in YS. Furthermore, at elevated temperatures, the YS of the alloys also increases with addition of Gd. At 250 °C and 300 °C, the addition of 3.0 wt% Gd increases the YS by 53.9 % and 81.4 %, respectively, compared to the Gd-free alloy. Thus, the addition of Gd can enhance the YS of the alloy. Moreover, the El of the alloys containing Gd is lower than the Gd-free alloy, at 250 °C and 300 °C. Detailed average data and standard deviations of the tensile properties of die-cast Mg1.6La1Ce-xGd alloys are listed in Table 2.

3.5. Fractured surface

See Fig. 12.

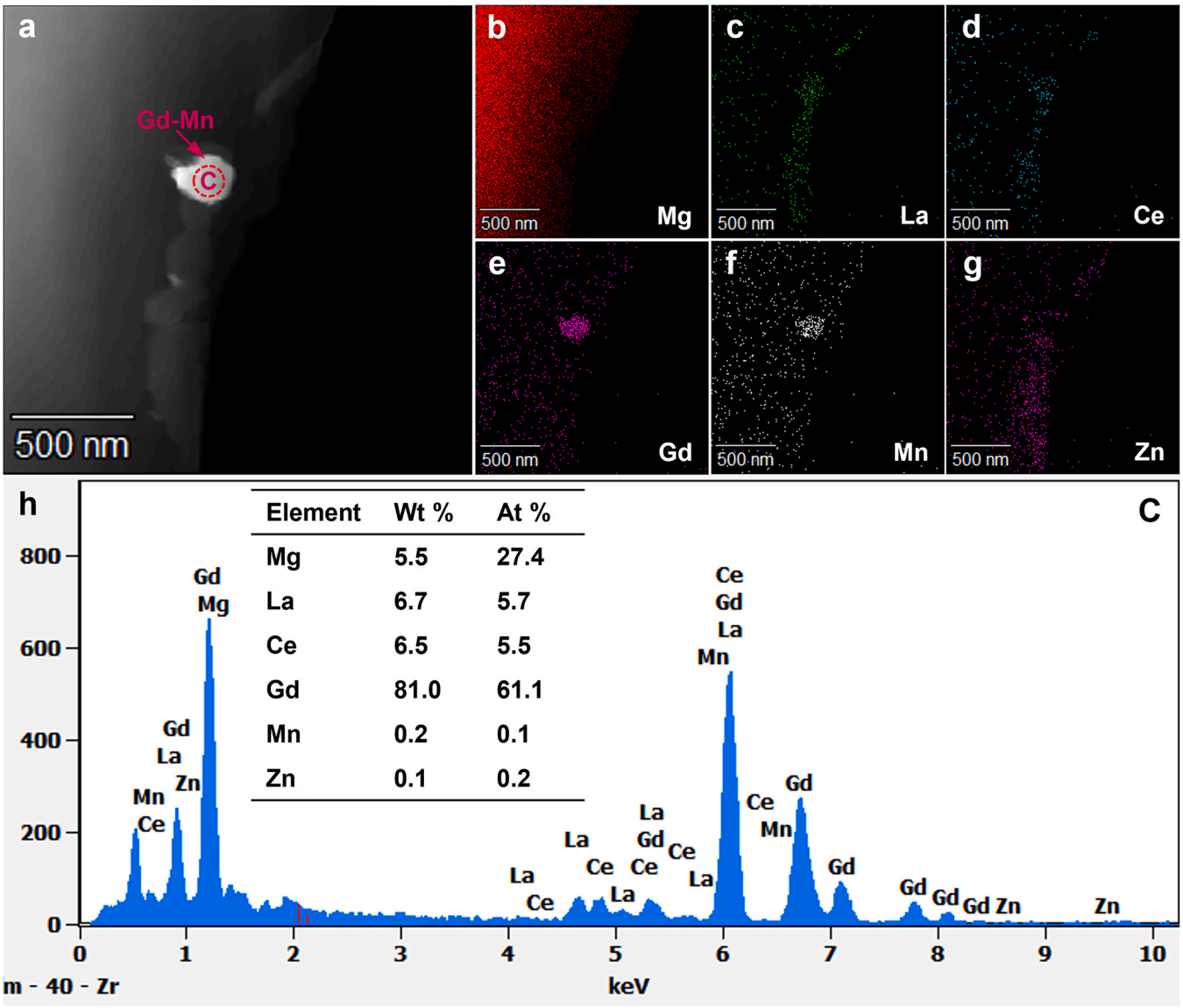

Fig. 9. TEM morphology and STEM-EDX results of the third minor blocky Gd-Mn intermetallic phase at grain boundaries of the die-cast Mg1.6La1Ce-3Gd alloy under as-cast condition. (a) STEM image; (b–g) STEM-EDX mapping of elements (b) Mg, (c) La, (d) Ce, (e) Gd, (f) Mn and (g) Zn in (a); (h) STEM-EDX result of the blocky Gd-Mn intermetallic phase marked by dashed circle in (a).

3.6. Microstructural evolution

The solidification process can demonstrate the evolution of microstructure. From the phase diagram of the Mg-Gd binary alloy, it can be seen that the eutectic reaction occurs at the position of Mg-4.53 at% Gd (Mg-23.5 wt% Gd) during solidification [9]. Therefore, the experimental alloys in this study should be hypo-eutectic.

Fig. 13a displays the calculated phase diagram of die-cast Mg1.6La1Ce-xGd alloys in the cross section of Mg1.6La1Ce with different Gd contents, using the Pandat CALPHAD software, and the possible phases present in the Gd-containing alloys are α-Mg, $Mg_{12}RE$ and Mg_5RE. In addition, the phase diagram indicates the formation of the Mg_5Gd phase at the onset of about 0.5 wt% Gd. Fig. 13b shows the calculated solidification curves of die-cast Mg1.6La1Ce-xGd alloys using the non-equilibrium Scheil model in Pandat software. The liquidus temperature and the temperature for the formation of $Mg_{12}RE$ phase decreases with the increased addition of Gd. The calculated $Mg_{12}RE$ phase agreed with the

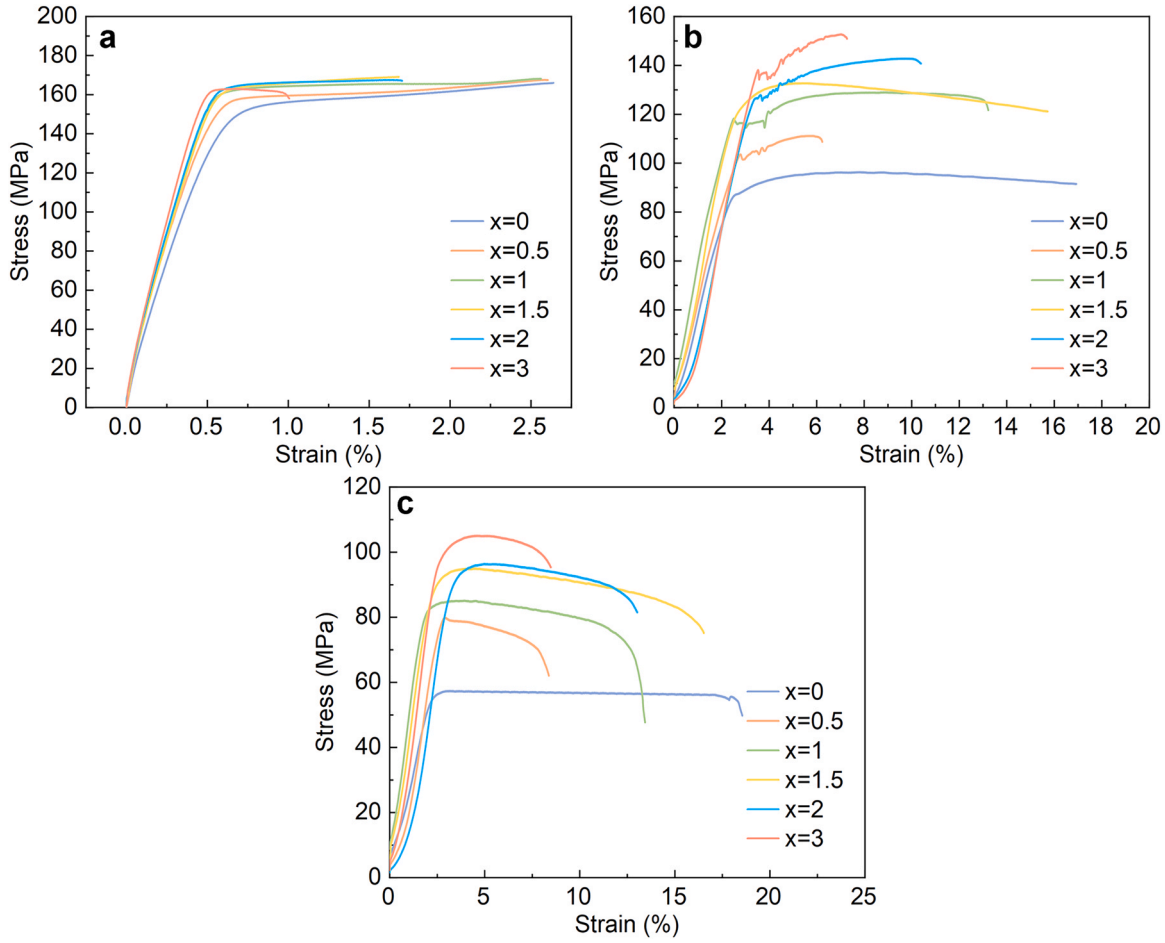

Fig. 10. Typical tensile stress-strain curve of die-cast Mg1.6La1Ce-xGd alloys in as-cast state at ambient temperature (20 °C), 250 °C and 300 °C. (a) 20 °C, (b) 250 °C, and (c) 300 °C.

experimental observations in Sections 3.2 and 3.3. However, the calculated Mg_5RE phase was not observed by the previous microstructure analysis. It may be due to the rapid solidification of HPDC, where the variation of the composition of the liquid and solid phases during the solidification of the alloy has deviated far from the equilibrium solidification [41,42]. Instead, the Mg_2Gd and Mg_3Gd phases with a higher solidification point formed in the liquid phase in the Gd-rich region at the beginning of solidification was retained at room temperature [28]. This explains the formation of Mg_2Gd and Mg_3Gd phases in the present alloys rather than the calculated Mg_5Gd phase.

3.7. Relationship between microstructure and mechanical properties

The addition of Gd improves the YS of the Mg1.6La1Ce alloy, as shown in Fig. 11 and Table 2. The strengthening mechanism of the Mg1.6La1Ce-xGd alloys can be expressed by grain strengthening (σ_{gb}), secondary phase strengthening ($\sigma_{Mg\text{-}RE}$) and solid solution strengthening (σ_{ss}) as follows [5,27,43]:

$$\sigma_{Mg1.6La1.0Ce-xGd} = \sigma_{gb} + \sigma_{ss} + \sigma_{Mg-RE} \quad (1)$$

The grain strengthening can be defined by the Hall-Petch relationship [44,45]:

$$\sigma_{gb} = \sigma_0 + Kd^{-\frac{1}{2}} \quad (2)$$

where d is the grain size and K is the material constant. According to Fig. 3a–f, the addition of Gd has very limited effect on the grain size of die-cast Mg1.6La1Ce-xGd alloys. Therefore, the addition of Gd hardly has effect on the increase or decrease of grain strengthening in Mg1.6La1Ce-xGd alloys.

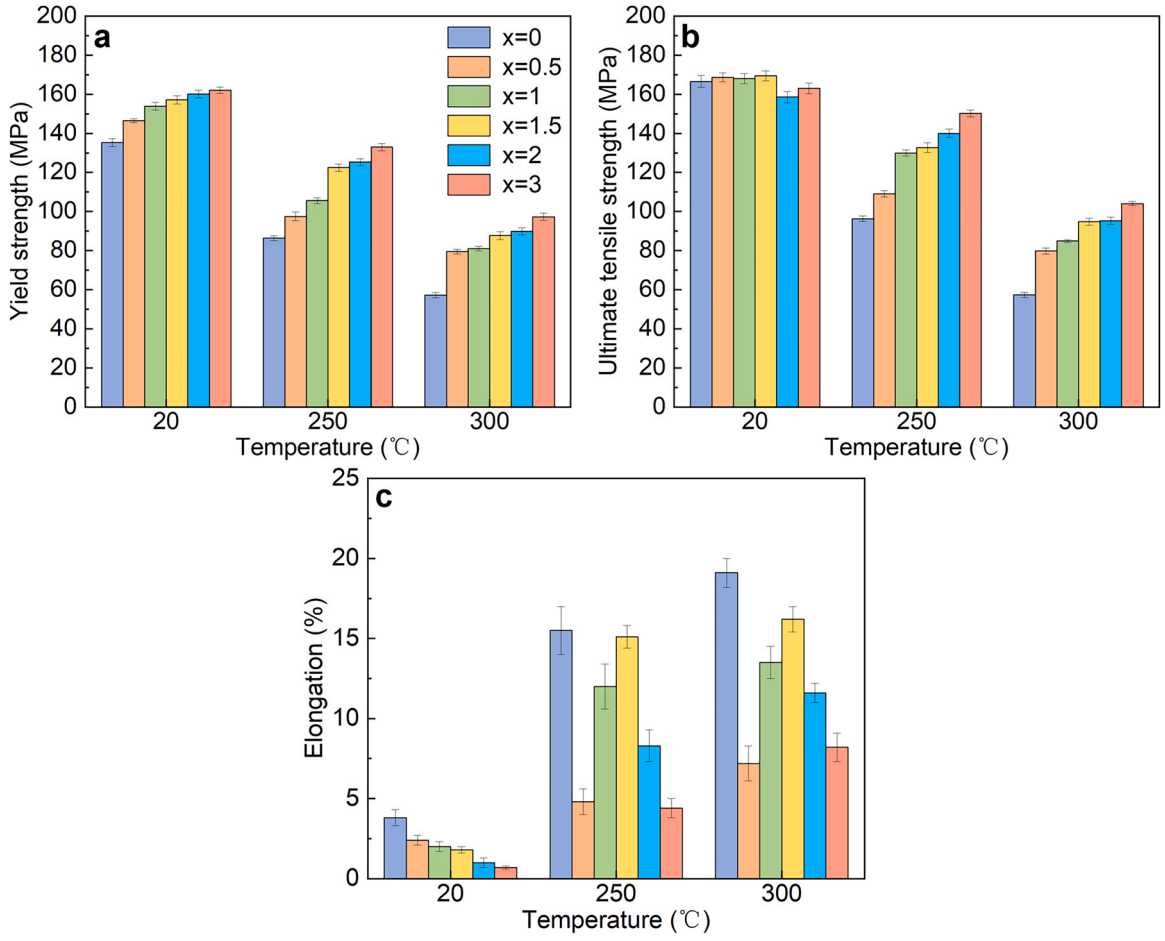

Fig. 11. Tensile properties of die-cast Mg1.6La1Ce-xGd alloys in as-cast state at ambient temperature (20 °C), 250 °C and 300 °C. (a) yield strength, (b) ultimate tensile strength, and (c) elongation.

Table 2
Tensile properties of the die-cast Mg1.6La1Ce-xGd alloys in the as-cast state.

Alloy	RT			250 °C			300 °C		
	YS (MPa)	UTS (MPa)	El (%)	YS (MPa)	UTS (MPa)	El (%)	YS (MPa)	UTS (MPa)	El (%)
x = 0	135.3 ± 2.1	166.6 ± 3.0	3.8 ± 0.5	86.4 ± 1.2	96.3 ± 1.4	15.5 ± 1.5	57.3 ± 1.3	57.4 ± 1.3	19.1 ± 0.9
x = 0.5	146.5 ± 1.0	168.7 ± 2.3	2.4 ± 0.3	97.5 ± 2.2	109.1 ± 1.7	4.8 ± 0.8	79.5 ± 1.2	79.8 ± 1.5	7.2 ± 1.1
x = 1.0	153.9 ± 1.9	168.0 ± 2.7	2.0 ± 0.3	105.6 ± 1.5	130.0 ± 1.5	12.0 ± 1.4	81.0 ± 1.2	84.9 ± 0.8	13.5 ± 1.0
x = 1.5	157.3 ± 2.1	169.4 ± 2.6	1.8 ± 0.2	122.5 ± 1.9	132.7 ± 2.4	15.1 ± 0.7	87.7 ± 2.0	94.8 ± 1.8	16.2 ± 0.8
x = 2.0	158.6 ± 2.0	160.3 ± 2.9	1.0 ± 0.3	125.3 ± 1.7	140.0 ± 2.2	8.3 ± 1.0	89.9 ± 2.3	95.3 ± 1.9	11.6 ± 0.6
x = 3.0	162.1 ± 1.6	163.0 ± 2.7	0.7 ± 0.1	133.0 ± 1.9	150.2 ± 1.8	4.4 ± 0.6	97.3 ± 1.9	104.1 ± 1.1	8.2 ± 0.9

According to the Mg-RE binary phase diagram, the equilibrium solubility of Gd (23.5 wt%) in the Mg matrix is much higher than that of La (0.23 wt%) and Ce (0.74 wt%) [9,46]. Solid solution strengthening can play a significant role in the strengthening of Gd-added Mg alloys. According to the EDS result of the Mg matrix in Fig. 5c, the solid solution content of Gd (1.2 wt%) is higher than the other elements, and the solid solution strengthening brought by Gd contributes considerably to the strengthening of the Mg1.6La1Ce-3Gd alloy.

The second phase strengthening originates from the hindrance of grain boundary dislocation slip by the formation of Mg-RE intermetallic phases at GBs. As shown in Fig. 3g, the volume fraction of

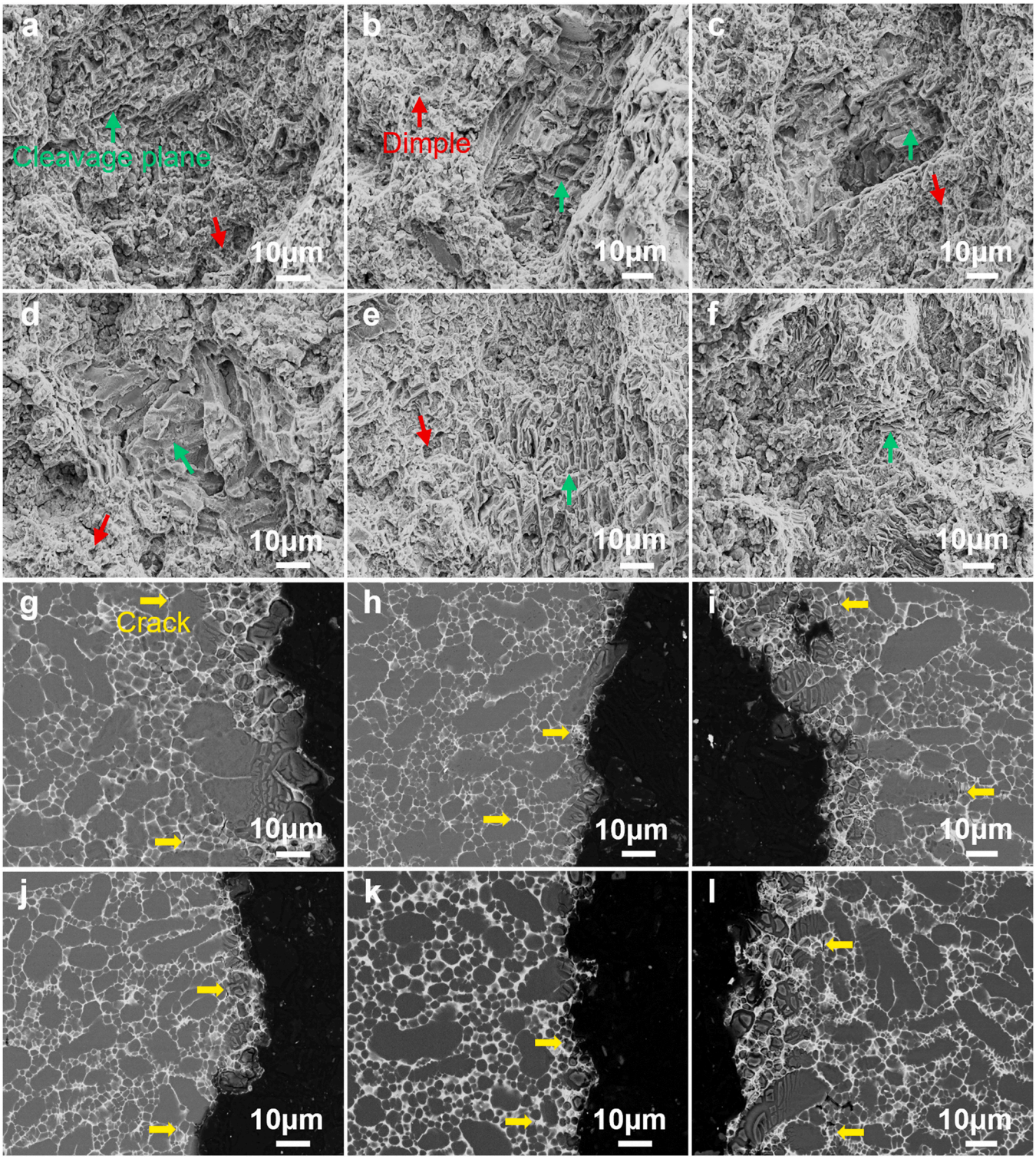

Fig. 12. (a–f) SE-SEM micrographs showing the fractured surface and (g–l) BSE-SEM micrographs of the sectioned surface near the fracture of the die-cast Mg1.6La1Ce-xGd alloys at ambient temperature. (a,g) x = 0, (b,h) x = 0.5, (c,i) x = 1.0, (d,j) x = 1.5, (e,k) x = 2.0, (f,l) x = 3.0.

intermetallic phases at GBs increases significantly from 11.7 % to 18.5 % with the addition of 3.0 wt% Gd. According to Figs. 2 and 4, both the major intermetallic phase ($Mg_{12}RE$) and the minor intermetallic phases (Mg_2Gd, Mg_3Gd, Gd-Mn) increase with the increased addition of Gd. The obvious increase in the volume fraction of intermetallic compounds indicates the considerable enhancement of second phase strengthening with Gd addition.

At elevated temperatures, the secondary phases distributed at the GBs can pin down the GBs and hinder dislocation movement, thus enhancing the strength of alloys [47]. The major skeleton-like

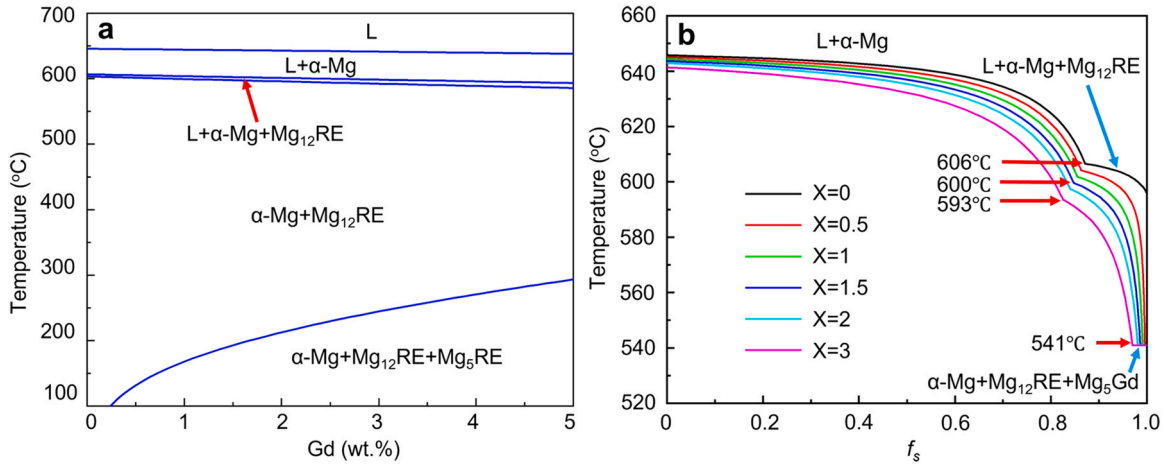

Fig. 13. (a) Calculated phase diagram of Mg1.6La1Ce-xGd alloys in the cross section of Mg1.6La1Ce with different Gd contents; (b) Calculated solidification curves of Mg1.6La1Ce-xGd alloys using the non-equilibrium Scheil model in the Pandat CALPHAD software.

$Mg_{12}RE$ intermetallic phase has a melting point of approximately 640 °C and good thermal stability [48]. According to the Mg-Gd phase diagram, the minor intermetallic phases Mg_2Gd and Mg_3Gd have the high melting points of 706 °C and 755 °C, respectively, and high thermal stability [49]. With the increased addition of Gd, the increase of thermally stable intermetallic phases contributes to the improvement of the strength of the Mg1.6La1Ce-xGd alloys at 250 °C and 300 °C.

4. Conclusions

The effects of Gd addition on the microstructure and tensile properties of the die-cast Mg1.6La1Ce-xGd alloys at ambient and elevated temperatures were investigated, and the main conclusions are as follows:

(1) The intermetallic compound at grain boundaries of the Gd-free alloy is the skeleton-like $Mg_{12}RE$ phase. In addition to the major $Mg_{12}RE$ phase, the addition of Gd leads to the formation of three minor Gd-containing intermetallic compounds at grain boundaries, i.e., the irregular-shaped Mg_2Gd phase, the needle-like Mg_3Gd phase and the blocky Gd-Mn phase. The domains of {011} twins were observed in the major $Mg_{12}RE$ intermetallic phase.
(2) The addition of Gd increases the volume fraction of both the major and minor intermetallic compounds at grain boundaries, while it has very limited effect on the grain size of the Mg matrix phase. With the increased addition of Gd from 0 wt% to 3 wt%, the total volume fraction of the intermetallic compounds increases significantly from 11.7 % to 18.5 %.
(3) The addition of Gd results in the increase of yield strength at both ambient and elevated temperatures. The YS of the Gd-free alloy is 135.3 MPa at ambient temperature and 57.3 MPa at 300 °C. The YS of the alloy with 3.0 wt% Gd is 162.1 MPa at ambient temperature and 97.3 MPa at 300 °C, which are increased by 19.8 % and 69.8 %, respectively, in contrast to the alloy without Gd addition.
(4) The increase in ambient yield strength can be mainly attributed to the increased secondary phase strengthening of intermetallic compounds at grain boundaries and the enhanced solid solution strengthening of Gd in Mg matrix. The increase of thermally stable intermetallic compounds $Mg_{12}RE$, Mg_2Gd and Mg_3Gd contribute to the increase of yield strength at elevated temperatures. The fracture mechanism of the Gd-containing alloys at ambient temperature is quasi-cleavage fracture.

CRediT authorship contribution statement

L. Feng: experimental conduction, data analysis and manuscript preparation. **X. Dong:** Supervision, conception, experimental design, results analysis, and manuscript editing. **Q. Cai:** Phase identification and data analysis. **B. Wang:** Supervision of experiments and discussion. **S. Ji:** Funding acquisition and manuscript proof.

Data Availability

No data was used for the research described in the article.

Declaration of Competing Interest

The authors declare that they have no known competing financial interests or personal relationships that could have appeared to influence the work reported in this paper.

Acknowledgement

The financial support from Innovate UK (Project reference: 10004694) are gratefully acknowledged.

References

[1] X. Peng, W. Liu, G. Wu, H. Ji, W. Ding, Plastic deformation and heat treatment of Mg-Li alloys: a review, J. Mater. Sci. Technol. 99 (2022) 193–206.
[2] Y. Fu, G.G. Wang, A. Hu, Y. Li, K.B. Thacker, J.P. Weiler, H. Hu, Formation, characteristics and control of sludge in Al-containing magnesium alloys: an overview, J. Magnes. Alloy. 10 (2022) 599–613.
[3] Y. Yang, X. Xiong, J. Chen, X. Peng, D. Chen, F. Pan, Research advances in magnesium and magnesium alloys worldwide in 2020, J. Magnes. Alloy. 9 (2021) 705–747.
[4] X. Dong, L. Feng, S. Wang, E.A. Nyberg, S. Ji, A new die-cast magnesium alloy for applications at higher elevated temperatures of 200–300°C, J. Magnes. Alloy. 9 (2021) 90–101.
[5] J. Rong, J.-N. Zhu, W. Xiao, X. Zhao, C. Ma, A high pressure die cast magnesium alloy with superior thermal conductivity and high strength, Intermetallics 139 (2021) 107350.
[6] N. Mo, Q. Tan, M. Bermingham, Y. Huang, H. Dieringa, N. Hort, M.-X. Zhang, Current development of creep-resistant magnesium cast alloys: a review, Mater. Des. 155 (2018) 422–442.
[7] X. Dong, L. Feng, S. Wang, G. Ji, A. Addad, H. Yang, E.A. Nyberg, S. Ji, On the exceptional creep resistance in a die-cast Gd-containing Mg alloy with Al addition, Acta Mater. 232 (2022) 117957.
[8] X. Dong, L. Feng, S. Wang, F. Wang, R. Ghasemi, G. Ji, E.A. Nyberg, S. Ji, A quantitative strategy for achieving the high thermal conductivity of die-cast Mg-Al-based alloys, Materialia 22 (2022) 101426.
[9] J.-F. Nie, Precipitation and hardening in magnesium alloys, Metall. Mater. Trans. A 43 (2012) 3891–3939.

[10] X. Dong, L. He, X. Huang, P. Li, Coupling analysis of the electromagnetic transport of liquid aluminum alloy during casting, J. Mater. Process. Technol. 222 (2015) 197–205.
[11] N. Li, C. Wang, M.A. Monclús, L. Yang, J.M. Molina-Aldareguia, Solid solution and precipitation strengthening effects in basal slip, extension twinning and pyramidal slip in Mg-Zn alloys, Acta Mater. 221 (2021) 117374.
[12] M. Celikin, A.A. Kaya, M. Pekguleryuz, Microstructural investigation and the creep behavior of Mg–Sr–Mn alloys, Mater. Sci. Eng. A 550 (2012) 39–50.
[13] S. Luo, L. Wang, J. Wang, G. Zhu, X. Zeng, Micro-compression of Al2Ca particles in a Mg-Al-Ca alloy, Materialia 21 (2022) 101300.
[14] H. Yong, S. Guo, Z. Yuan, Y. Qi, D. Zhao, Y. Zhang, Phase transformation, thermodynamics and kinetics property of Mg90Ce5RE5 (RE = La, Ce, Nd) hydrogen storage alloys, J. Mater. Sci. Technol. 51 (2020) 84–93.
[15] X. Dong, L. He, X. Huang, P. Li, Effect of electromagnetic transport process on the improvement of hydrogen porosity defect in A380 aluminum alloy, Int. J. Hydrogen Energy 40 (2015) 9287–9297.
[16] S.V.S. Prasad, S.B. Prasad, K. Verma, R.K. Mishra, V. Kumar, S. Singh, The role and significance of magnesium in modern day research-a review, J. Magnes. Alloy. 10 (2022) 1–61.
[17] W. Qudong, C. Wenzhou, Z. Xiaoqin, L. Yizhen, D. Wenjiang, Z. Yanping, X. Xiaoping, M. Mabuchi, Effects of Ca addition on the microstructure and mechanical properties of AZ91magnesium alloy, J. Mater. Sci. 36 (2001) 3035–3040.
[18] Y. Nakaura, A. Watanabe, K. Ohori, Effects of Ca,Sr additions on properties of Mg-Al based alloys, Mater. Trans. 47 (2006) 1031–1039.
[19] B. Hu, W.-J. Zhu, Z.-X. Li, S.B. Lee, D.-J. Li, X.-Q. Zeng, Y.S. Choi, Effects of Ce content on the modification of Mg2Si phase in Mg-5Al-2Si alloy, J. Magnes. Alloy. (2021).
[20] J. Zhang, Z. Leng, M. Zhang, J. Meng, R. Wu, Effect of Ce on microstructure, mechanical properties and corrosion behavior of high-pressure die-cast Mg–4Al-based alloy, J. Alloy. Compd. 509 (2011) 1069–1078.
[21] J. Zhang, J. Wang, X. Qiu, D. Zhang, Z. Tian, X. Niu, D. Tang, J. Meng, Effect of Nd on the microstructure, mechanical properties and corrosion behavior of die-cast Mg–4Al-based alloy, J. Alloy. Compd. 464 (2008) 556–564.
[22] S. Zhu, M.A. Easton, T.B. Abbott, M.A. Gibson, J.-F. Nie, The influence of individual rare earth elements (La, Ce, or Nd) on creep resistance of die-cast magnesium alloy AE44, Adv. Eng. Mater. 18 (2016) 932–937.
[23] M. Pekguleryuz, M. Celikin, Creep resistance in magnesium alloys, Int. Mater. Rev. 55 (2013) 197–217.
[24] S. Zhu, M.A. Easton, T.B. Abbott, J.-F. Nie, M.S. Dargusch, N. Hort, M.A. Gibson, Evaluation of magnesium die-casting alloys for elevated temperature applications: microstructure, tensile properties, and creep resistance, Metall. Mater. Trans. A 46 (2015) 3543–3554.
[25] C.J. Bettles, K. Venkatesan, J.F. Nie, Microstructure and mechanical properties of MEZ casting alloy, Mater. Sci. Forum 419–422 (2003) 273–278.
[26] S. Gavras, M.A. Easton, M.A. Gibson, S. Zhu, J.-F. Nie, Microstructure and property evaluation of high-pressure die-cast Mg–La–rare earth (Nd, Y or Gd) alloys, J. Alloy. Compd. 597 (2014) 21–29.
[27] Y. Xu, F. Gensch, Z. Ren, K.U. Kainer, N. Hort, Effects of Gd solutes on hardness and yield strength of Mg alloys, Prog. Nat. Sci.: Mater. Int. 28 (2018) 724–730.
[28] H. Miao, H. Huang, S. Fan, J. Tan, Z. Wang, W. Ding, G. Yuan, Nanoscale precipitations in deformed dilute alloying Mg-Zn-Gd alloy, Mater. Des. 196 (2020) 109122.
[29] L. Xiao, Y. Zhong, C.-p Chen, M.-m Wuliu, T.-k Luo, L.-b Liu, K. Lin, Isothermal section of Mg–Nd–Gd ternary system at 723 K, Trans. Nonferrous Met. Soc. China 24 (2014) 777–782.
[30] J.F. Nie, K. Oh-ishi, X. Gao, K. Hono, Solute segregation and precipitation in a creep-resistant Mg–Gd–Zn alloy, Acta Mater. 56 (2008) 6061–6076.
[31] M.-X. Zeng, R.-N. Wang, B.-Y. Tang, L.-M. Peng, W.-J. Ding, Elastic and electronic properties of tI26-type Mg12RE (RE = Ce, Pr and Nd) phases, Modell. Simul. Mater. Sci. Eng. 20 (2012) 035018.
[32] X. Hua, Q. Yang, D. Zhang, F. Meng, C. Chen, Z. You, J. Zhang, S. Lv, J. Meng, Microstructures and mechanical properties of a newly developed high-pressure die casting Mg-Zn-RE alloy, J. Mater. Sci. Technol. 53 (2020) 174–184.
[33] L. Feng, X. Dong, Q. Cai, B. Wang, S. Ji, Effect of Nd on the microstructure and mechanical properties of Mg-La-Ce alloys at ambient and elevated temperatures, J. Mater. Eng. Perform. (2022).
[34] M. Suzuki, T. Kimura, J. Koike, K. Maruyama, Strengthening effect of Zn in heat resistant Mg–Y–Zn solid solution alloys, Scr. Mater. 48 (2003) 997–1002.
[35] P. Manfrinetti, K.A. Gschneidner, Phase equilibrium in the La-Mg (0–65at% Mg) and Gd-Mg systems, J. Less-Common Met 123 (1986) 267–275.
[36] X.-F. Gu, T. Furuhara, L. Chen, P. Yang, Study on the planar segregation of solute atoms in Mg-Al-Gd alloy, Scr. Mater. 150 (2018) 45–49.
[37] J.D. Robson, S.J. Haigh, B. Davis, D. Griffiths, Grain boundary segregation of rare-earth elements in magnesium alloys, Metall. Mater. Trans. A 47 (2015) 522–530.
[38] C. He, Z. Li, H. Chen, N. Wilson, J.F. Nie, Unusual solute segregation phenomenon in coherent twin boundaries, Nat. Commun. 12 (2021) 722.
[39] N. Mo, I. McCarroll, Q. Tan, A. Ceguerra, J. Cairney, H. Dieringa, Y. Huang, B. Jiang, F. Pan, M. Bermingham, M.-X. Zhang, Roles of Nd and Mn in a new creep-resistant magnesium alloy, Mater. Sci. Eng. A 779 (2020) 139152.
[40] R. Pei, S.K. Woo, S. Yi, T. Al-Samman, Effect of solute clusters on plastic instability in magnesium alloys, Mater. Sci. Eng. A 835 (2022).
[41] T. Le, Q. Wei, J. Wang, P. Jin, M. Chen, J. Ma, Effect of different casting techniques on the microstructure and mechanical properties of AE44-2 magnesium alloy, Mater. Res. Express 7 (2020) 116513.
[42] M.-w Wu, L. Hua, S.-m Xiong, Modeling studies on divorced eutectic formation of high pressure die cast magnesium alloy, China Foundry 15 (2018) 58–65.
[43] X. Dong, S. Amirkhanlou, S. Ji, Formation of strength platform in cast Al-Si-Mg-Cu alloys, Sci. Rep. 9 (2019) 9582.
[44] R. Zhao, W. Zhu, J. Zhang, L. Zhang, J. Zhang, C. Xu, Influence of Ni and Bi microalloying on microstructure and mechanical properties of as-cast low RE LPSO-containing Mg–Zn–Y–Mn alloy, Mater. Sci. Eng. A 788 (2020) 139594.
[45] X. Dong, Y. Zhang, S. Ji, Enhancement of mechanical properties in high silicon gravity cast AlSi9Mg alloy refined by Al3Ti3B master alloy, Mater. Sci. Eng. A 700 (2017) 291–300.
[46] K.R. Athul, U.T.S. Pillai, A. Srinivasan, B.C. Pai, A review of different creep mechanisms in Mg alloys based on stress exponent and activation energy, Adv. Eng. Mater. 18 (2016) 770–794.
[47] Z.-Z. Jin, X.-M. Cheng, M. Zha, J. Rong, H. Zhang, J.-G. Wang, C. Wang, Z.-G. Li, H.-Y. Wang, Effects of Mg17Al12 second phase particles on twinning-induced recrystallization behavior in Mg-Al-Zn alloys during gradient hot rolling, J. Mater. Sci. Technol. 35 (2019) 2017–2026.
[48] J. Xie, J. Zhang, Z. You, S. Liu, K. Guan, R. Wu, J. Wang, J. Feng, Towards developing Mg alloys with simultaneously improved strength and corrosion resistance via RE alloying, J. Magnes. Alloy. 9 (2021) 41–56.
[49] L. Zhu, Q. Li, Q. Zhang, X. Chen, Dynamic precipitation in Mg–8.08Gd–2.41Sm–0.30Zr alloy during hot compression, Materials 11 (2018).